BULLETIN OF THE POLISH ACADEMY OF SCIENCES
TECHNICAL SCIENCES, Vol. 66, No. 2, 2018
DOI: 10.24425/119064

Influence of slim obstacle geometry on the flow and heat transfer in microchannels

M. KMIOTEK* and A. KUCABA-PIĘTAL

Department of Fluid Mechanics and Aerodynamics, Rzeszow University of Technology,
12 Powstańców Warszawy Av., Rzeszów 35-959, Poland

Abstract. This paper presents a computational study on hydrodynamic and heat transfer characteristics of the laminar flow inside a rectangular 2D microchannel of height *H,* which includes a slim micro obstacle of height *h* and width *w* placed on the lower wall of the channel. The Reynolds number varies between 20 and 200. Three different values of height *h* and two different shapes of the slim obstacles: triangular and rectangular one, are considered. Thus, a total of 24 geometrical configurations of fluid flow are analyzed. Fluid flow equations are solved using the commercial CFD package of ADINA R&D, Inc. 9.1. Detailed analysis of the fluid velocity field and streamlines is carried out to investigate the flows in recirculation zone behind the obstacle. Results obtained show that the rectangular obstacle caused larger vortex formation in fluid flow. For flows with larger value of the (h/H) ratio, an increase in the value of loss coefficient factors is observed. Meanwhile, the increased Reynolds number causes the vortex zone behind the rectangular obstacle to be larger than behind the triangular one.

Key words: microchannels, obstacle, finite element method.

1. Introduction

Thanks to miniaturization processes, microchannels are now used in cooling systems of many technical devices. Because of their small size, the flow inside them is laminar, which results in slow heat exchange. In order to intensify the heat exchange, the flow must be disturbed, for example by means of introducing obstacles.

The use of obstacles on the walls increases heat and mass transfer, as already discussed macrochannel literature [5, 9, 10, 14, 15, 17, 25]. When moving the concept of obstacle into microchannels, it is important to know how the obstacle shape and its geometrical parameters will disturb the flow the most in microscale.

Obstacles on the wall disturb the flow and introduce vortex zones behind the obstacle. This is an important range of problems to be noted during the construction and operation of different micro devices (i.e. flow identification, temperature distribution, pressure loss, vortex zones), where the solution improves the device's efficiency. In micro devices laminar flow very often occurs because the Reynolds number decreases with the reduction microchannel hydraulic diameter [23].

In the construction of micro-technical devices, microchannels of different dimensions are used, depending on the area of applicability of the device. Usually the height of the microchannel is the smallest linear dimension. Channels with the smallest linear dimension, which is smaller than 1 mm and greater than 1 μm, are called microchannels [12, 22]. Channels with a larger size are called millichannels.

The microchannel obstacle is defined as an obstacle having a height greater than 6% of the microchannel, otherwise it is treated as a roughness, for example in [6–8, 11, 13, 21, 26].

Microchannels with obstacles are widely used in heat exchangers, solar and geothermal heating systems, aviation, cooling systems for electronic devices, especially computer processors, micromixers as well as chemical and biological microsystems.

A number of investigators have explored the mechanisms of flow and heat transfer caused by obstacles mounted onto channel walls, depending on the size and geometry of the flow field, characterized by Reynolds Re number and the h/H – (obstacle/channel) aspect ratio value. The aspect ratio value is defined as a quotient of obstacle height to the height of the channel.

Błoński et al. [4] studied fluid flow in a microchannel with a single obstacle numerically and experimentally. The results indicate that deformation of flow field in the microchannel was observed for fluid flow characterized by $\mathrm{Re} > 10$.

Stogiannis et al. [24] presented numerical and experimental studies for fluid flow in microchannel with a single obstacle. Flows which alter obstacle geometry and Re were studied. The obstacles had different heights, i.e. $h/H = 0.4$ or $h/H = 0.8$, and width $w/h = 16$. Reynolds number varied from 100 to 1600. The results show that the length of the vortex zone back to the obstacle depends on the value of the parameters mentioned above.

Seo et al. [20] investigated fluid flow in microchannels with obstacles of different shapes: rectangular, triangular and oval ones. The results showed that the triangular shape of the obstacle had most influence on fluid and heat flow.

Baheri Islami et al. [2, 3] investigated two-dimensional flow of fluid in a microchannel with obstacles, for $\mathrm{Re} = 5$; $\mathrm{Re} = 20$ and $\mathrm{Re} = 50$ values, respectively. The obstacles had different

*e-mail: kmimal@prz.edu.pl

Manuscript submitted 2017-11-13, revised 2018-01-28, initially accepted for publication 2018-02-03, published in April 2018.

heights and were characterized by different aspect ratios of $h/H = 0.33$; 0.5 and 0.66. The results showed that parameters such as obstacle height and Reynolds number affect the length of the vortex zones behind the obstacles. Results from the above-mentioned papers concern obstacles for which value of aspect ratio w/h, which is defined as a quotient of obstacle width to height, by far exceeds the value of 1.

Kmiotek et al. [15] studied the influence of different geometries of the obstacle. The influence of an obstacle of triangular and rectangular shape on water flow in two dimensional channels was checked. Reynolds number equaled 20. The numerical results on fluid flow in the microchannel where obstacles were mounted onto the wall show that it is strongly influenced by geometrical parameters of obstacle as well as by the shape and length of the vortex zones behind the obstacles.

A review of literature studies on flow properties in microchannels with obstacles mounted onto walls indicates that the presence of obstacles in microchannels during laminar flow of fluid causes additional fluid movement, which affects mass and heat transfer, indirectly increasing the efficiency of fluid heat transfer to the channel wall. The efficiency of flow systems such as heat exchangers depends on flow separation in internal flow caused by vortices formation at the back of each mounted obstacle. Almost all studies presented in the literature on the flow and heat transfer in microchannels with obstacles mounted onto the walls concern obstacles characterized by aspect ratio $w/h \geq 1$. There are only a few papers devoted to investigating fluid flow through microchannels with slim obstacles, which are defined by parameter values of $w/h < 0.5$. Applicability of slim obstacles in microchannels is important for at least two reasons: material savings and possibility of flow disturbance control caused by slim obstacle movement, forced, for instance, by an external electric field [4, 18, 24].

This work presents systematic investigations of two-dimensional fluid flow in a microchannel with a mounted slim obstacle. We focus on the influence of geometric parameters characterizing a single slim obstacle on the recirculation zone back to the obstacle in a microchannel and heat transfer characteristics. The problem is studied numerically. The influence of parametric changes in the obstacles' geometry, shape and with different flow rates are examined to establish transfer fundamental effects and provide practical results. The influence of governing parameters on streamlines and length of the zone of recirculation back to the obstacle are also analyzed. However pressure drop is calculated, too. It is shown that specific choices of certain governing parameters, such as obstacle height or shape, can result in significant changes in flow field.

2. Problem formulation

Two-dimensional, steady, laminar fluid flow in a microchannel with the slim obstacle mounted onto the lower wall is considered (Fig. 1). Microchannels consist of two parallel plates of length L situated at distance H. Slim obstacle of height h and width w is placed inside the channel on the lower wall. The distance of the obstacle from the inlet of the channel is l. Steady, laminar flow enters the microchannel with uniform velocity V.

Fluid flow in microchannel can be described by equations representing the conservation laws of mass and heat transfer and the linear momentum. In the Cartesian coordinate system, this is written as:

$$\frac{\partial v}{\partial x} + \frac{\partial u}{\partial y} = 0 \tag{1}$$

$$\rho\left(v\frac{\partial v}{\partial x} + u\frac{\partial u}{\partial y}\right) = -\frac{\partial p}{\partial x} + \mu\left(\frac{\partial^2 v}{\partial x^2} + \frac{\partial^2 u}{\partial y^2}\right) \tag{2}$$

$$\rho\left(v\frac{\partial v}{\partial x} + u\frac{\partial u}{\partial y}\right) = -\frac{\partial p}{\partial y} + \mu\left(\frac{\partial^2 v}{\partial x^2} + \frac{\partial^2 u}{\partial y^2}\right) \tag{3}$$

$$\rho\left(v\frac{\partial T}{\partial x} + u\frac{\partial T}{\partial y}\right) = k\left(\frac{\partial^2 T}{\partial x^2} + \frac{\partial^2 T}{\partial y^2}\right) \tag{4}$$

where p is the fluid pressure, ρ is the fluid density, μ is the fluid dynamic viscosity coefficient, v, u are components of the velocity vector $\boldsymbol{V} = (v, u)$, T stands for temperature and k is the thermal conductivity coefficient.

The problem of fluid flow and heat transfer in a microchannel with an obstacle of different shapes was considered. The microchannel geometry is shown in Fig. 1.

Boundary conditions along the entire solution domain must be specified.

Constant velocity and temperature is specified at the inlet to the channel while the stream rise gradients of the velocity components at the outlet are assumed to be zero. Velocity satisfies non-slip conditions along the fluid/solid interfaces.

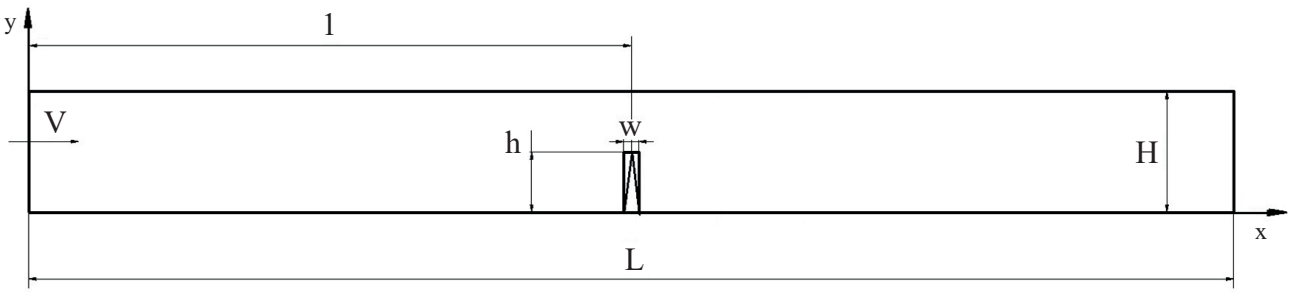

Fig. 1 Computational domain

The applied boundary conditions are as follows:
1) Inflow: x = 0, 0 ≤ y ≤ H, v = V, $u = 0$, $T = T_{in}$;
2) Outflow: x = L, 0 ≤ y ≤ H;
3) Non-slip velocity conditions at the wall, i.e.: y = 0, u = v = 0; y = H, $u = v = 0$;
4) Non-slip velocity conditions at the obstacle, i.e.: $u = 0$, $v = 0$;
5) Temperature at the walls and at the obstacle, i.e.: $T = T_w$;

Equations (1–4) were solved for the following parameter values: L = 0,008 m, H = 400 μm, l = 0,004 m, h = 100, 200 and 300 μm, w = 10, 20 and 50 μm, T_{in} = 20°C, T_w = 60°C. Obstacles of different triangular or rectangular shapes were considered.

Fluid flow was characterized by the Reynolds number, which was defined as follows:

$$Re = \frac{\rho V H}{\mu} \tag{5}$$

where ρ is fluid density and μ denotes the fluid dynamic viscosity coefficient. The working fluid is water. The physical properties of water used in the calculations are: $\rho = 998.3$ kg/m^3, $\mu = 0.001$ Pa · s. The non-dimensional parameters' values which characterize the geometry of the flow in the microchannel with an obstacle used in the calculations are presented in Table 1.

Table 1
Obstacle parameter values

No.	h [μm]	h/H	w [μm]	w/h
1	100	0.25	10	0.1
2	100	0.25	20	0.2
3	100	0.25	50	0.5
4	200	0.5	10	0.05
5	200	0.5	20	0.1
6	200	0.5	50	0.25
7	300	0.75	10	0.033
8	300	0.75	20	0.067
9	300	0.75	50	0.17

Heat transfer was characterized by the Nusselt number, which was defined as follows:

$$Nu = \frac{h_x H}{k} \tag{6}$$

where h_x is the heat transfer coefficient and k is the thermal conductivity coefficient of the fluid.

The heat transfer coefficient is defined as

$$h_x = \frac{q_w}{T_w - T_f} \qquad h_x = -k\frac{\frac{\partial T}{\partial n}}{T_f - T_w} \tag{7}$$

where q_w is the wall heat flux, T_w is wall temperature, T_f fluid temperature, and $\partial T/\partial n$ provides the temperature gradient component normal for the wall.

3. Numerical solution and validation

Numerical calculations of flow field and heat transfer in the microchannels were performed for:
- nine different geometries of the flow field (characterized in Table 1),
- two different obstacle shapes: triangular and rectangular one,
- four Reynolds numbers: 20, 50,100, 200.

The governing equations (1–4) were solved numerically using the Adina CFD & FSI solver [1], which uses the finite element method. For the microchannels with triangular obstacles an unstructured mesh based on the 2D quadrilateral element and 2D triangular grid elements, consisting of about 129 700 nodes and 128 000 elements, was created. For the microchannels with rectangular obstacles, a structured mesh based on the 2D quadrilateral element grid elements, consisting of about 80 361 nodes and 79 200 elements, is used. Besides, prior to performing the analysis, grid sensitivity analysis was performed. The value of the grid convergence index [19] was thus calculated.

$$GCI = \frac{F_s}{r^p - 1}\left|\frac{u_{h2} - u_{h1}}{u_{h1}}\right| \cdot 100 \tag{8}$$

where F_s – the safety factor, $F_s = 1.25$ [18], u_{h1}, u_{h2} – the chosen parameter (max. velocity in the x plane), h_1, h_2 – the number of finite elements for two types of grids, respectively, r – the density factor, p – the order of convergence, $p = 2$.

For a grid in which the length of the finite element was 5 μm, a CGI of less than 0.1% was obtained.

The numerical model has been validated using the experimental data obtained by use of the micro Particle Image Velocimetry (μPIV) method to measure 2D velocity fields in the millichannels as in [4].

Based on the similarity rule of flows, a millichannel was designed (scale 5:1). An obstacle of height $h = H/2$, was placed on the lower wall. The obstacle was of a rectangular shape. The μPIV measurements of velocity field were performed at Reynolds number Re = 50. Velocity vector fields near the obstacle obtained from μPIV data and numerical calculations are outlined in Fig. 2.

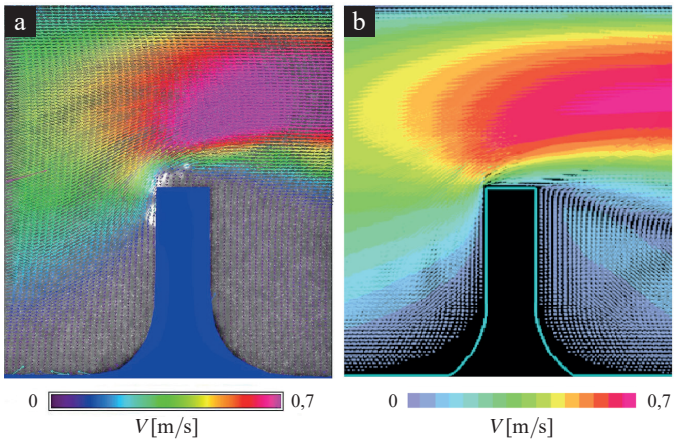

Fig. 2. Velocity vector field near obstacle, $h/H = 0.5$, Re = 50. a) μPIV data, b) numerical calculations

The velocity profiles from μPIV data and numerical calculations are presented in Fig. 3. The results show good compatibility for numerical and experimental results. They differ by no more than 3%, where the difference between the experimental data (d_e) and numerical data (d_n) was defined as: 100% $(d_e - d_n)/d_n$.

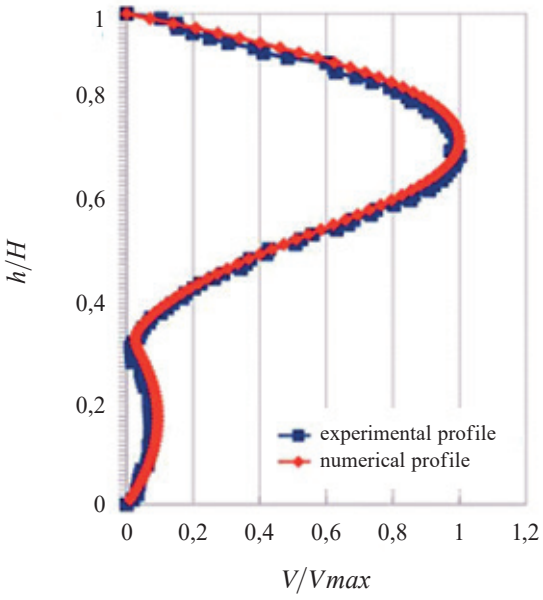

Fig. 3. Velocity profiles from μPIV data and from numerical calculations for the rectangular shape of obstacle, Re = 50

4. Results an discussions

Calculations of the flow field were performed for various values of parameters listed in Table 1, for differing obstacle geometry:

- the obstacle height aspect ratio (h/H) and the obstacle width aspect ratio (w/h),
- various inlet velocity.

Moreover, the values of loss coefficient ξ for slim obstacles and heat transfer characteristics were calculated.

4.1. Effect of obstacle height aspect ratio (h/H) on flow field. The water flow distributions in the microchannel with slim obstacles were compared in order to visualize how their shapes influence the fluid field. The obstacle (triangular and rectangular) with width $w = 10$ μm and the heights of aspect ratio $h/H = 0.25$, $h/H = 0.5$, $h/H = 0.75$ have been investigated. Figure 4 shows the representation of flow field streamlines for rectangular and triangular obstacles which were obtained for different values of the obstacle height aspect ratios. Differences in streamline contours for flows past the obstacles of rectangular and triangular shape for Re = 20 and for the obstacle height aspect ratio $h/H = 0.25$, $h/H = 0.5$, $h/H = 0.75$ are observed. There is a recirculation zone behind the obstacles.

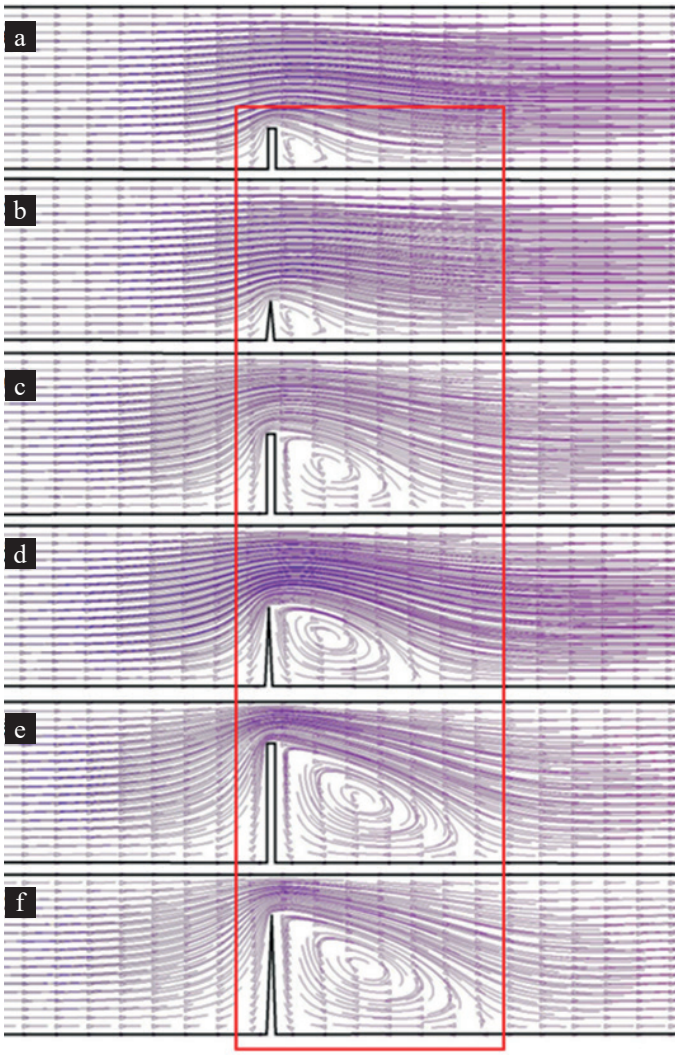

Fig. 4. Streamlines of water flows in microchannels with a rectangular (a, c, e) and triangular (b, d, f) obstacle, for Re = 20 a, b – $h/H = 0.25$; c, d – $h/H = 0.5$; e, f – $h/H = 0.75$

Vorticity is measured by means of circulation, however, the vortex can be characterized by the length of the recirculation zone. This method was used by Zhao et al. [27] to characterize the vortex on the back of an obstacle, and we follow it in the present paper. The length of recirculation zone (denoted by d_w) was identified as the distance from the obstacle to the vortex closure (Fig. 5). The recirculation zone aspect ratio d_w/H was also calculated, i.e. the length of recirculation zone was divided by microchannel height H.

Figure 5 presents streamlines in the flow field past triangular and rectangular obstacles. As expected, it can be clearly observed that the recirculation zone becomes longer with increasing value of the obstacle height aspect ratio. The values calculated are as follows: for the rectangular obstacle: for $h/H = 0.25$ it is $d_w/H = 0.38$, for $h/H = 0.5$ it is $d_w/H = 0.89$, for $h/H = 0.75$ it is $d_w/H = 1.3$ and for the triangular obstacle: for $h/H = 0.25$ it is $d_w/H = 0.39$, for $h/H = 0.5$ it is $d_w/H = 0.94$, and for $h/H = 0.75$ it is $d_w/H = 1.3$.

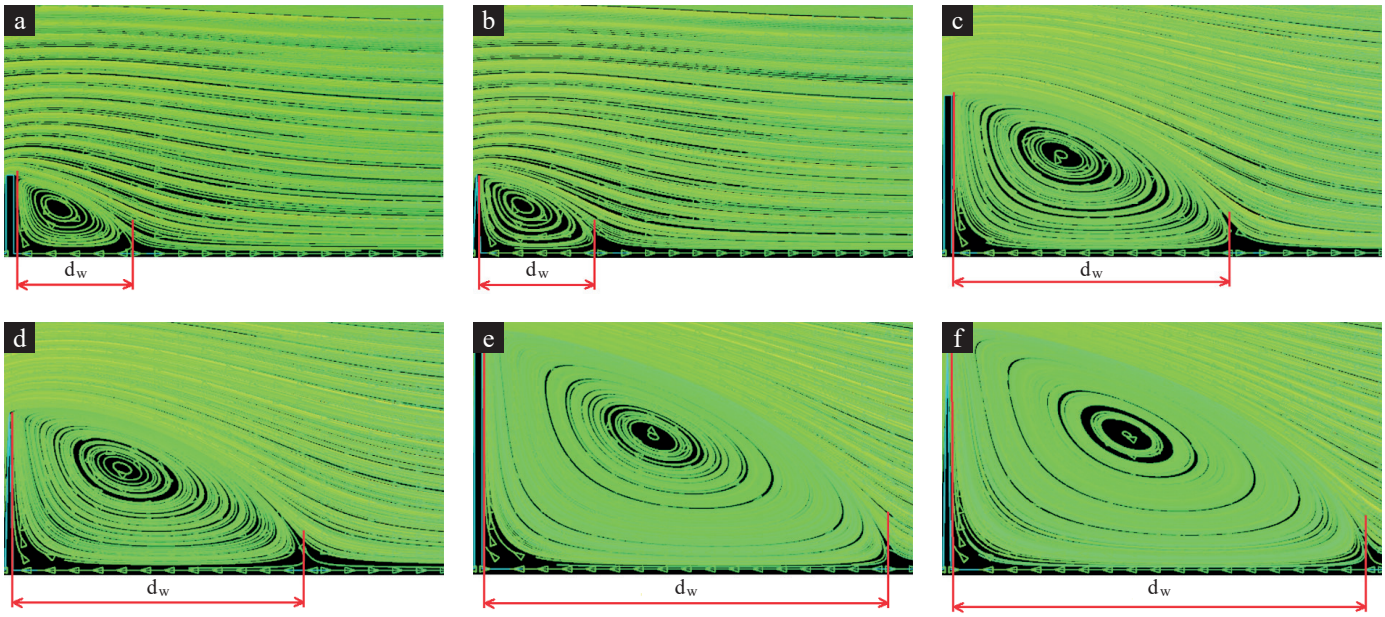

Fig. 5. Length of the recirculation zone d_w behind the rectangular (a, c, e) and triangular (b, d, f) obstacle, for Re = 20; a, b – $h/H = 0.25$; c, d – $h/H = 0.5$; e, f – $h/H = 0.5$

Results show that the recirculation zone length d_w increases with obstacle height. However, for flows in the microchannel with the triangular obstacle, the recirculation zone length d_w is longer than in the microchannel with the rectangular one.

4.2. Effect of obstacle width aspect ratio (w/h) on flow field. To investigate the effect of an obstacle width, the velocity profiles were outlined. The obstacle (triangular and rectangular) with height $h = 0.5H$ and characterized by different values of the width aspect ratio, i.e. $w/h = 0.05$, $w/h = 0.1$, $w/h = 0.5$, were investigated. The flow in the channel at the inlet had a velocity of $V = 0.05$ m/s (Re = 20). Figure 6 shows the velocity profiles in five planes oriented perpendicularly to the microchannel walls situated as: $x_1 = l - H$, $x_2 = l$, $x_3 = l + H$, $x_4 = l + 2H$, $x_5 = l + 3H$, for three different values of the rectangular obstacle width aspect ratio. The results show that flow separation depends massively on the obstacle width aspect ratio w/h. At distance x_3 the water velocity profile deforms, loses symmetry, and the maximum velocity profile moves above half of the height of the microchannel. For ratio $h/H = 0.5$, the change in the width of the obstacle has no significant effect on the flow for distance x_4. The length of recirculation zone d_w decreases with obstacle width (for $w/h = 0.025$ it is $d_w/H = 0.38$, for $w/h = 0.05$ it is $d_w/H = 0.35$, for $w/h = 0.125$ it is $d_w/H = 0.33$).

Results show that the effect of the obstacle width aspect ratio w/h for triangular and rectangular obstacles on flow field disturbance is much more apparent in the case of rectangular obstacles mounted on the microchannel wall. The reduced aspect ratio w/h increased the average flow velocity in microchannels by 4% for $w/h = 0.05$ and by 8% for $w/h = 0.1$, versus $w/h = 0.25$. Increasing obstacle width aspect ratio w/h of the triangular obstacles decreases the mean flow velocity non-significantly (up to 2% difference).

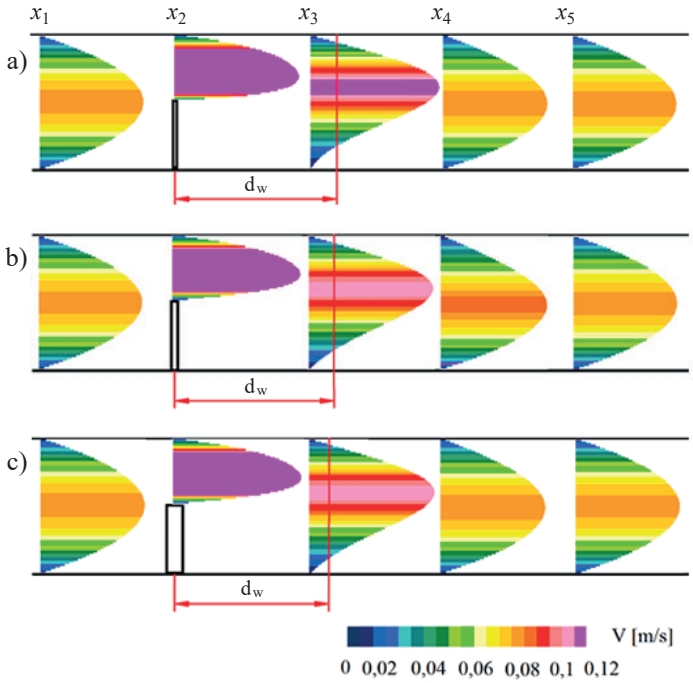

Fig. 6. Velocity profiles V of water flows in the microchannel with the rectangular obstacle, Re = 20; a – $w/h = 0.05$; b – $w/h = 0.1$; c – $w/h = 0.25$

4.3. Effect of Reynolds number on the velocity field. In Fig. 7 water velocity vectors in the microchannel are presented as depending on Reynolds number values, which varied from 20 to 200. The obstacles (triangular and rectangular) with width $w = 50$ μm and the height aspect ratio $h/H = 0.25$ were taken into account.

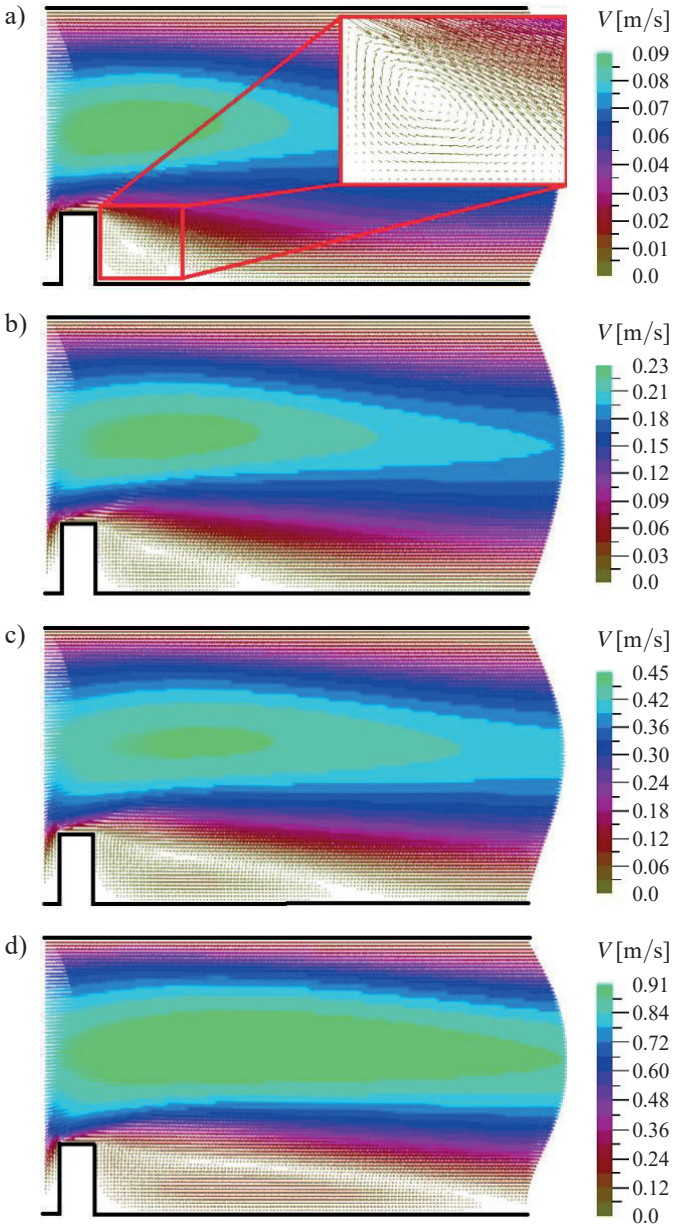

Fig. 7. Velocity vector fields in microchannels with the rectangular obstacle, $w/h = 0.5$, $h/H = 0.25$; a) Re = 20; b) Re = 50; c) Re = 100; d) Re = 200

The results show that the length of the recirculation zone d_w increases with the increase of the Reynolds number. Calculations are shown for water flows in microchannels with a rectangular slim obstacle mounted on the wall: for Re = 20 it is $d_w/H = 0.33$, for Re = 50 it is $d_w/H = 0.61$, for Re = 100 it is $d_w/H = 1$, and for Re = 200 it is $d_w/H = 1.53$. For water flows in the microchannel with a triangular obstacle mounted on the wall results of calculations are as follows: for Re = 20 it is $d_w/H = 0.33$, for Re = 50 it is $d_w/H = 0.62$, for Re = 100 it is $d_w/H = 1$, and for Re = 200 it is $d_w/H = 1.26$. It was observed that for the Reynolds number Re = 200 the length of recirculation zone d_w behind the rectangular obstacle is larger than for the triangular obstacle.

4.4. Loss coefficient ξ calculations for slim obstacles. Knowledge of energy loss coefficients ξ is needed for the hydraulic flow systems calculations. Value of the loss coefficient depends on the type of obstacle and its geometry. The loss coefficient ξ value can be predicted as:

$$\xi = \frac{2\Delta P}{\rho V^2} \tag{9}$$

where: ΔP is the pressure drop and V stands for average fluid velocity in the microchannel.

According to experimental study [26], we calculated the values of loss coefficient ξ for slim obstacle depending on its geometry and shape from the following formula:

$$\xi = \frac{2 \cdot [2 \cdot (p_2 - p_3) - (p_1 - p_4)]}{\rho V^2} \tag{10}$$

where: V is average velocity in the microchannel, $p_1 - p_4$ – pressure values in the corresponding cross sections oriented perpendicularly to the microchannel walls situated at: p_1 at a distance of $4H$, p_2 at a distance of $2H$ in front of the obstacle, p_3 at a distance of 2H, and p_4 at a distance of 4H behind the obstacle, respectively.

Values of the loss coefficient ξ were determined from formula (10) for various geometries of rectangular and triangular slim obstacles and are presented in Table 2. The results show that the ξ value for the obstacle increases with the height of the obstacle. The increase in the width of the obstacle causes an increase in value of the loss factor ξ for both rectangular and triangular obstacles.

Table 2
Values of the loss coefficient ξ for rectangular (Rr) and triangular (Tr) slim obstacles

h/H	w/h	$\xi(Rr)$	$\xi(Tr)$
0.25	0.1	1.2	1.1
0.25	0.2	1.18	1.1
0.25	0.5	1.28	1.09
0.50	0.05	7.08	7.08
0.50	0.1	7.11	7.11
0.50	0.25	7.37	6.98
0.75	0.033	44.91	45.84
0.75	0.067	44.69	45.66
0.75	0.17	47.04	45.08

4.5. Heat transfer characteristics. The heat transfer distributions in the microchannel with slim obstacles were compared in order to visualize how their shapes influence the temperature field. Figure 8 shows of the temperature fields in the microchannel with rectangular and triangular obstacles. They were obtained for different values of the obstacle height aspect ratios. Differences in temperature fields for flows past the obstacles of rectangular and triangular shape for Re = 20 and for the obstacle height aspect ratio $h/H = 0.25$, $h/H = 0.5$, $h/H = 0.75$ are observed.

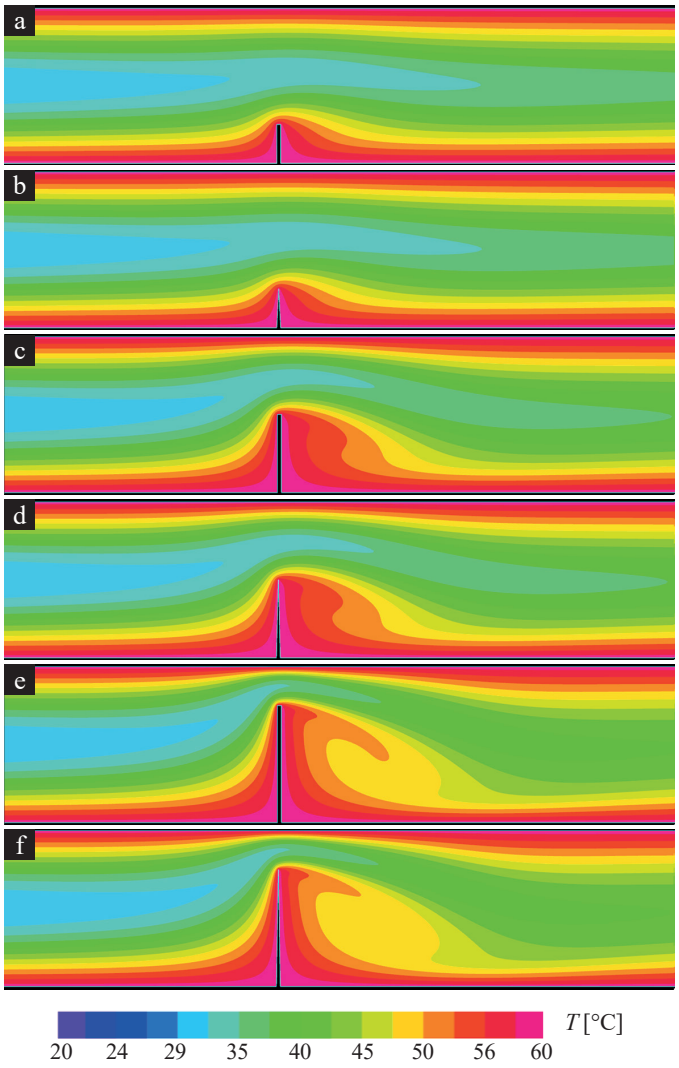

Fig. 8. Temperature distributions [°C] in microchannels with a rectangular (a, c, e) and triangular (b, d, f) obstacle, for Re = 20; a, b) $h/H = 0.25$; c, d) $h/H = 0.5$; e, f) $h/H = 0.75$, $w = 10$ μm

The results show that temperature distribution depends on the obstacle height aspect ratio and shape of the obstacle. The temperature distribution zone behind the obstacles is similar to the fluid flow disturbances presented in Fig. 4.

Figure 9 shows the local Nusselt numbers in five planes oriented perpendicularly to the microchannel walls, distributed as follows: $X_1 = l - 4H$, $X_2 = l - 2H$, $X_3 = l$, $X_4 = l + 2H$, $X_5 = l + 4H$. Variations of local Nusselt numbers with length of the microchannel L for a triangular and rectangular obstacle for three different values of the obstacle height aspect ratio and a smooth channel for Reynolds number (Re = 20) are presented.

The results show higher local Nusselt numbers for the microchannels with obstacles as compared with a smooth channel. Table 3 summarizes their percentage difference values. The value of local Nusselt number for height aspect ratio $h/H = 0.25$, $h/H = 0.5$ is slightly higher for rectangular obstacles than the triangular ones. Only for height aspect ratio

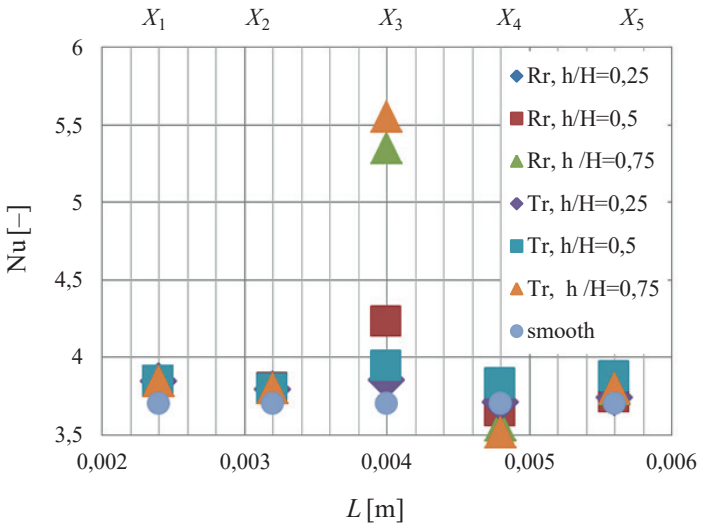

Fig. 9. Variation of Nu [-] with length of the microchannel L [m] for the triangular (*Tr*) and rectangular (*Rr*) obstacle

$h/H = 0.75$ the value of local Nusselt numbers at distance X_4 is lower for the microchannels with the rectangular obstacle than for the microchannels with the triangular one. At the distance $X_3 = 0.004$ [m] the local Nusselt number achieves maximum for different values of the obstacle height aspect ratios and shape of obstacle, which is related to the maximum flow velocity and the reduced distance between the microchannel wall and the top of the obstacle. Compared to the smooth microchannel, the local increase of Nu number for the microchannel with the obstacle raises the average value of Nu number, which leads to the increase of the net value of heat transfer.

Table 3
Percentage differences in Nusselt numbers in the channels with an obstacle $(\mathrm{Nu_o})$ and without $(\mathrm{Nu_{sm}})$, $\%\mathrm{Nuo} = \left((\mathrm{Nu_o} - \mathrm{Nu_{sm}})/\mathrm{Nu_{sm}}\right) \cdot 100\%$,

h/H	*Planes*	$\%\mathrm{Nu_o}$ (*Rr*)	$\%\mathrm{Nu_o}$ (*Tr*)
0,25	X_1	3,78	3,78
0,25	X_2	2,43	2,43
0,25	X_3	14,32	4,05
0,25	X_4	–1,62	0,27
0,25	X_5	2,7	1,08
0,5	X_1	3,78	3,78
0,5	X_2	2,7	2,43
0,5	X_3	14,2	6,49
0,5	X_4	–1,35	3,51
0,5	X_5	1,08	4,59
0,75	X_1	3,78	3,78
0,75	X_2	2,7	2,7
0,75	X_3	44,59	50
0,75	X_4	–3,78	–5,13
0,75	X_5	2,43	2,7

5. Conclusions

The effect of the wall-mounted obstacle on fluid flow was studied numerically to answer the question of how the slim obstacle of different shapes, i.e. triangular and rectangular ones, disturbs the flow. A parametric study revealed the effect of design parameters on the recirculation zone behind the obstacle. The main observations from the analysis are listed below.

The increase of obstacle height increases the length of recirculation zone and the length of recirculation zone is longer for the triangular obstacle than for the rectangular one.

1. The increase of obstacle width reduces the length of recirculation zone.
2. The increase of Reynolds number values increases the length of recirculation zone, but the length of recirculation zone behind the rectangular obstacle is longer than behind the triangular one.
3. The increase of obstacle height increases the value of loss coefficient ξ for the obstacles. The increase of obstacle width increases the value of loss factor ξ for both rectangular and triangular obstacles.
4. The rectangular obstacle causes larger vortex formation in fluid flow.
5. Microchannels with obstacles exhibit higher heat transfer than the smooth channels.
6. The increase of obstacle's height increases the heat transfer, the value of loss coefficient ξ for the obstacles and the length of recirculation zone.

The results obtained for a single obstacle form the basis for designing microchannels with slim obstacles in the channel. They allow to choose optimum spacing between obstacles depending on flow velocity. At the same time, they enable the determination of pressure loss in the microchannels with slim obstacles.

References

[1] Adina R&D, Inc. *Theory and Modeling Guide, Volume III,* ADINA CFD&FSI, Report ARD, 2015.
[2] S. Baheri Islami, B. Dastvareh, and R. Gharraei, "An investigation on the hydrodynamic and heat transfer of nanofluid flow, with non-Newtonian base fluid, in micromixers", *International Journal of Heat and Mass Transfer* 78 (2014) 917–929.
[3] S. Baheri Islami, B. Dastvareh, and R. Gharraei, "Numerical study of hydrodynamic and heat transfer of nanofluid flow in microchannels containing micromixer", *International Communications in Heat and Mass Transfer* 43, 146–154 (2013).
[4] S. Błoński, P. Domagalski, M. Dziubiński, and T.A. Kowalewski, "Hydro-dynamically modified seeding for micro-PIV", *Arch. Mech.* 63 (2) 163–182 (2011).
[5] L. Chai, G.D. Xia, and H.S. Wang, "Numerical study of laminar flow and heat transfer in microchannel heat sink with offset ribs on sidewalls", *Applied Thermal Engineering* 92, 32–41, (2016).
[6] M. Chen, B.Y. Cao, and Z.Y. Guo, "Micro/nano-scale fluid flow on structured surfaces", ICNMM 2008–62023.
[7] G. Croce and P.D'Agaro, "Numerical simulation of roughness effect on microchannel heat transfer and pressure drop in laminar flow", *J. Phys. D: Appl. Phys.* 38, 1518–1530 (2005).
[8] G. Gamrat, M. Favre-Marinet, and D. Asendrych, "Conduction and entrance effects on laminar liquid flow and heat transfer in rectangular microchannels", *International Journal of Heat and Mass Transfer* 48, 2943–2954 (2005).
[9] S. Gareh, "Numerical heat transfer in rectangular channel with mounted obstacle", *International Letters of Chemistr, Physics and Astronomy* 19 (2), 111–119 (2014).
[10] Q. Gravndyan, O.A. Akbari, D. Toghraie, A.Marzban, R. Mashayekhi, R. Karimi, and F. Pourfattah, "The effect of aspect ratios of rib on the heat transfer and laminar water/TiO2 nanofluid flow in a two-dimensional rectangular microchannel", *Journal of Molecular Liquids* 236, 254–265 (2017).
[11] H. Herwig, D. Gloss, and T. Wenterodt, "Flow in channels with rough walls-old and new concepts", ICNMM 2008–62064.
[12] S. Kandikar and S. Gerimella, *Heat Transfer and Fluid Flow in Minichannels and Microchannels*, Elsevier Ltd., 2006.
[13] M.H. Khadem, M. Shams, and S. Hossainpour, "Numerical simulation of roughness effects on flow and heat transfer in microchannels", *International Communication in Heat and Mass Transfer* 36, 69–77 (2009).
[14] Z. Kheirandish, S.A Gandjalikhan Nassab, and M. Vakilian, "Second law analysis of forced convective cooling in a channel with heated wall mounted obstacle", *Journal of Electronics Cooling and Thermal Control* 3, 101–110 (2013).
[15] M. Kmiotek and A. Kucaba-Pietal, "Finite Element Method as a modern tool for engineering calculations, [in:] *Issues of Contemporary Computing Science*, ed. T. Lewandowski, PWSTE Jaroslaw, 97–110, 2016.
[16] T. Ma, Q. Wang, M. Zeng, Y. Chen, Y. Liu, and V. Nagarajan, "Study on heat transfer and pressure drop performances of ribbed channel in the high temperature heat exchanger", *Applied Energy* 99, 393–401 (2012).
[17] H.F. Ozop, Y. Varol, and D.E. Alnak, "Control of heat transfer and fluid flow using a triangular bar in heated bloks located in a channel", *International Communications in Heat and Mass Transfer* 36, 878–885 (2009).
[18] A.G. Passos, V.-A. Chatzieleftheriou, and A.A. Mouza, "Casson fluid flow in a michrochanel containing a flow distrub rib", *Chemical Engineering Science* 14, 229–237 (2016).
[19] P.J. Roache, *Verification and Validation in Computational Science and Engineering*, Hermosa Publishers, Albuquerque, NM, 1998.
[20] H.S. Seo and Y.J. Kim, "A study on the mixing characterics in a hybrid type microchannel with various obstacle configurations, *Materials Research Bulletin* 17, 948–2951 (2012).
[21] S. Shen, J.L. Xu, J.J. Zhou, and Y. Chen, "Flow and heat transfer in microchannels with rough wall surface", *Energy Conversion and Management* 47, 1311–1325 (2006).
[22] K.I. Sotowa, A. Yamamoto, K. Nakagawa, and S. Sugiyama, "Indentation an baffles for improving mixing ratr in deep microchannel reactors", *Chemical Engineering Journal* 167, 490–495 (2011).
[23] M. Steinke, and S. Kandlikar, "Single-phase liquid friction factors in microchannels, *International Journal of Thermal Science* 45, 920060, 1073–1083.
[24] I.A. Stogiannis, A.D. Passos, A.A. Mouza, S.V. Paras, V. Pěnkavová, and J. Tihon, "Flow investigation in a microchannel with a flow disturbing rib", *Chemical Engineering Science* 119 65–76 (2014).
[25] Y.T. Yang and C.Z. Hwang, "Calculation of turbulent flow and heat transfer in a porous-baffled channel", *International Journal of Heat and Mass Transfer* 46, 771–780 (2003).
[26] C. Zhang and Y. Chen, "Effects of roughness elements on laminar flow and heat transfer in microchannels", *Chemical Engineering and Processing* 49, 1188–1192 (2010).
[27] J. Zhao, S.Huang and L. Gong, "Numerical studies on geometric features of microchannel heat sink with pin fin structure", *4th Micro and Nano Flows Conference,* UCL, London (2014).